C. R. Mecanique 341 (2013) 181–190

Contents lists available at SciVerse ScienceDirect

Comptes Rendus Mecanique

www.sciencedirect.com

Combustion, flow and spray dynamics for aerospace propulsion

Analysis of limit cycles sustained by two modes in the flame describing function framework

Analyse de cycles limites impliquant deux modes dans le cadre de l'équivalent harmonique pour les flammes

Frédéric Boudy [a,b,*], Daniel Durox [a,b], Thierry Schuller [a,b], Sébastien Candel [a,b]

[a] *CNRS, UPR 288 – laboratoire EM2C, 92290 Châtenay-Malabry, France*
[b] *École centrale Paris, 92290 Châtenay-Malabry, France*

ARTICLE INFO

Article history:
Available online 16 January 2013

Keywords:
Combustion instabilities
Describing Function
Heterodyning
Limit cycles

Mots-clés :
Instabilités de combustion
Méthode de l'équivalent harmonique
Hétérodynage
Cycles limites

ABSTRACT

The Flame Describing Function (FDF) framework, developed for the nonlinear instability analysis of combustors, has been validated more recently in a generic configuration comprising an upstream manifold, an injection unit and a flame tube. This system featuring a wide variety of dynamical phenomena, is used here to explore a new range of self-sustained flame oscillations. Depending on the geometry, the system exhibits stable or variable amplitude limit cycles. In the first case, oscillations have an essentially constant amplitude and are well retrieved with the FDF framework, whereas in the second case, limit cycles feature different types of amplitude unsteadiness and require some further consideration. The present article is concerned with one type of unstable oscillation in which a regular period modification occurs in the presence of two modes, leading to frequency heterodyning. It is found from the FDF analysis that such oscillations sustained by two modes may occur when there is an overlap between modes corresponding to super and subcritical bifurcations. An additional condition which has to be fulfilled to obtain this behavior is inferred from experiments.

RÉSUMÉ

La méthode de l'équivalent harmonique (FDF), développée pour l'analyse non-linéaire des instabilités de combustion, a été récemment validée dans une configuration générique comportant un élément d'alimentation, un dispositif d'injection et un tube à flamme. Ce système caractérisé par des comportements dynamiques très variés, est utilisé pour analyser une nouvelle gamme d'oscillations de flamme. Suivant la géométrie, le système fait apparaître plusieurs types de cycles limites. Dans un premier cas, les oscillations ont une amplitude approximativement constante. Dans un second cas, l'amplitude du cycle limite varie de façon instationnaire. L'étude traite d'un régime d'oscillation de ce dernier type impliquant deux modes et induisant une modification régulière de la période faisant aussi apparaître un hétérodynage de fréquence. Cette situation peut être envisagée dans le cadre de la méthode FDF lorsque les taux de croissance de deux modes, correspondant

* Corresponding author at: CNRS, UPR 288 – laboratoire EM2C, 92290 Châtenay-Malabry, France.
E-mail address: frederic.boudy@ecp.fr (F. Boudy).

1631-0721/$ – see front matter
http://dx.doi.org/10.1016/j.crme.2012.10.014

à des bifurcations supercritique et sous-critique, se chevauchent. Une deuxième condition nécessaire à ce comportement est déduite à partir des expériences.

1. Introduction

Dynamical flame modeling constitutes a key component in the prediction of thermo-acoustic oscillations. It has already been shown that the flame response can be characterized with a Flame Transfer Function (FTF) and that this provides an initial insight in the combustor dynamics. However, the oscillation time history and amplitude level cannot be deduced from a linear analysis. In addition, it is well known that unstable combustion may occur even if the system is predicted to be linearly stable. Issues in linear analysis are illustrated for example in the case of a generic unconfined flame configuration [1] or in a more complex situation of a premixed turbulent combustor [2]. Data gathered in this last case are used to determine unstable ranges of a gas turbine and predict staging effects. In general linear analysis provides indications on the unstable range and reveals benefits of geometrical and operating parameter changes but it is also found that there is a gap between instability prediction and experiments confirming that flame nonlinearity needs to be taken into account.

This point was recognized in early studies and most notably in the area of liquid rocket combustion instability. Studies of unsteady ducted flames typical of afterburner configurations also indicated that nonlinearity was responsible for amplitude saturation observed in experiments [3]. It was shown in a simpler configuration that energy could be transferred to harmonics as the amplitude of oscillation increased [4]. The flame nonlinearity was considered for example by Dowling [5] to explain the saturation of oscillations observed by Langhorne [6] in the case of a flame anchored on a central bluff body placed in a ducted low-Mach-number premixed flow. The analysis relied on the Describing Function (DF) methodology borrowed from control theory in combination with a representation of flame gain saturation when the flow reversed. An improved kinematic model for the flame was later devised [7] and the describing function analysis was carried out providing successful predictions of the unstable amplitude and frequency. The describing function also designated as the "harmonic equivalent" is well suited to processes which are essentially linear but comprise a nonlinear component. It uses a quasi-linear response function to define the nonlinear element by only considering the first harmonic component in the output. It was shown more recently that a unified framework using a "Flame Describing Function" (FDF) [8] provides reliable predictions of frequency and amplitude of self-sustained combustion oscillations. This was demonstrated on a multiple flame burner initially considered in [1]. The model accounts for the nonlinearities of the flame in both gain and phase. It was shown that the FDF could be used to determine the growth rate of various modes of oscillation as a function of amplitude. It was then possible to determine a bifurcation diagram providing the frequency and amplitude of the different oscillations observed experimentally by changing the size of the feeding manifold. The experiment reported in [8] also revealed hysteresis and triggering points which were well retrieved by calculations. More recently, the FDF method has been used to determine the regimes of instability of a turbulent swirling flame [9] and predict the amplitude levels of limit cycle oscillations. In this latter study, the bifurcation parameter was the flame tube but this configuration, characterized by an upstream Helmholtz resonator, did not feature triggering or hysteresis. The FDF was used in [10] to predict triggering in a generic system comprising an upstream manifold, a multiple injection system and a flame tube. It was also shown that the frequency evolution with the amplitude could be retrieved. However, further examination of experimental results indicated that certain parametric ranges were not well rendered with the FDF methodology. Problems arise when the limit cycle amplitude cannot be considered constant but evolves as a function of time. In some cases the amplitude modulations are irregular giving rise to "Galloping limit cycles" (GLCs), a term borrowed from civil engineering [11] to define cable oscillations with varying amplitude. In the present case the limit cycle amplitude is modulated in a more regular fashion and the oscillation is sustained by two modes and will be designated in what follows as TMLC (Two Modes Limit Cycle). This behavior was not observed in the unconfined situation investigated in [8] but TMLCs arise in the generic system considered in the present study in a limited range of the bifurcation parameter.

In the analysis and calculation of thermo-acoustic coupling it is generally assumed that the amplitude and frequency are fixed. It is known however that limit cycles are not always locked on an amplitude at a fixed frequency. This is for example found in the premixed laboratory combustor used by Sterling [12] where quasi-periodic oscillations were identified and linked to the interaction of two acoustic eigenmodes. More recent experimental investigations in a multiple flame combustor equipped with a perforated plate comprising seven orifices have also revealed variable amplitude limit cycles [13,14] which were uncovered by examining different combustion chamber lengths.

The present work complements our previous investigation of a multiple injection combustor [15]. It specifically deals with TMLCs appearing in this system in which the multiple flame region is confined in a tube. This variable amplitude oscillation state, which can be qualified as "buzzing-blown" combustion due to its auditive signature, is analyzed in the special case where two different modes coexist. The test rig is briefly presented in Section 2. Experimental results are reported in Section 3. The situation is examined with the FDF framework in Section 4. It is shown that TMLCs arise in a region where the domains of instability of two modes overlap.

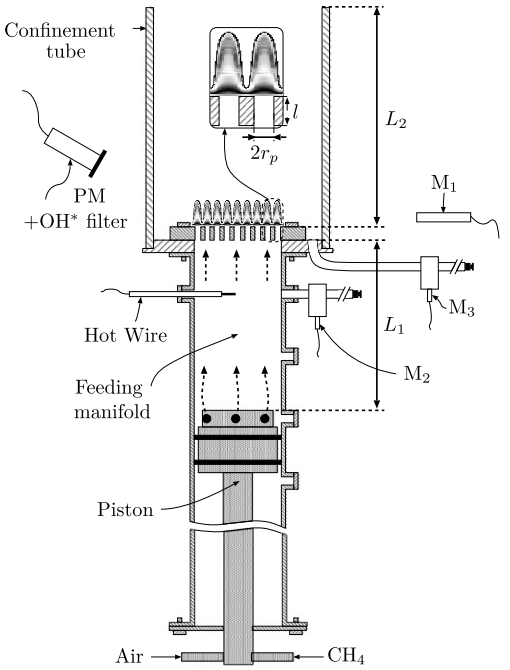

Fig. 1. Experimental setup and diagnostic devices used to characterize self-sustained instabilities.

2. Burner geometry and operating conditions

The experimental setup used in the present work is sketched in Fig. 1. Except for a thickened perforated plate, it features the elements used in our previous investigations [10,15]. An adjustable feeding manifold length L_1 of diameter $D_1 = 0.07$ m allows injection of a methane/air mixture. This premixture flows through a piston used to change the feeding manifold length L_1 and delivers the fresh stream through a peripherically holed flat head. Flames are anchored on a perforated plate. The thickness of this plate is $l = 15$ mm and there are $N = 421$ holes of diameter $d_p = 2$ mm. A confinement tube of length $L_2 = 0.10$ m and diameter $D_2 = 0.13$ m encloses the combustion region. Regimes of combustion are characterized at limit cycle by means of velocity and pressure measurements. Heat release rate fluctuation is estimated by measuring free radicals emissions. The mass flow rate is set here to $\dot{m} = 4.71 \times 10^{-3}$ kg s^{-1} for an equivalence ratio of $\phi = 1.03$, providing a thermal power of 13.3 kW. This flow induces a bulk velocity of $U_b = 3.1$ m s^{-1} in each perforated plate channel.

Three microphones are used for pressure measurements. The first one M_1 is located 24.5 cm away from the burner axis. The second M_2 is connected to a waveguide which is plugged in the same section as a hot wire located 3 cm below the perforated plate. Microphone M_3 is also connected on a waveguide to scan the pressure evolution in the flame region. Free radical light emission is measured by a photodiode equipped with an OH* filter. This sensor placed at a distance from the flame tube collects the light radiated by the flame region.

Another set of experiments has been used to characterize the flame response subjected to harmonic velocity perturbations of different amplitudes. The flow is excited by a loudspeaker placed at the bottom of the burner. It modulates the flow from 0 to 1300 Hz in a relative amplitude range (u_{rms}/U_b) swept from 6 to 77% where U_b indicates the bulk flow velocity in the perforation. Loudspeaker efficiency bounds the amplitude and frequency range covered in these experiments. Nevertheless, thanks to the forced flame response measurements and the burner self-sustained combustion oscillations, the flame response is interpolated and extrapolated in missing areas. This flame response linked to a set of Flame Transfer Function at different amplitudes is designated as the Flame Describing Function (FDF). It is defined as the ratio of the relative heat release rate fluctuations to the relative velocity fluctuations:

$$\mathcal{F}(\omega_r, u_{rms}/U_b) = \frac{\dot{Q}'/\bar{\dot{Q}}}{u_{rms}/U_b} = G(\omega_r, u_{rms}/U_b) e^{i\varphi(\omega_r, u_{rms}/U_b)} \tag{1}$$

where ω_r indicates the angular forcing frequency and u_{rms} the root mean square velocity fluctuation measured by LDV at 0.7 mm above one hole of the perforated plate.

3. Experimental analysis

The system described in Section 2 is now used to obtain the bifurcation diagram of self-sustained combustion oscillations for a confinement tube length $L_2 = 0.10$ m by varying the feeding manifold length L_1 between 0.11 m and 0.77 m. The

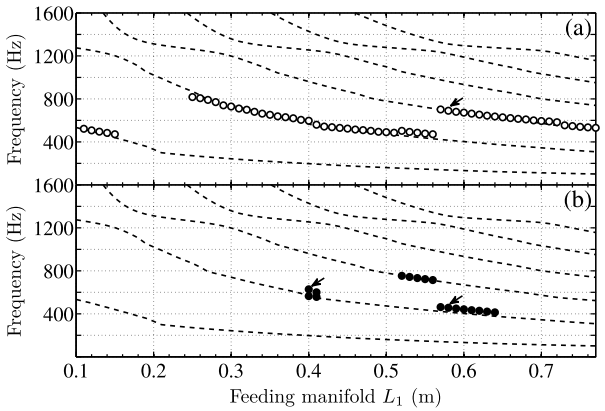

Fig. 2. Frequency evolution by increasing the feeding manifold length L_1 for the $L_2 = 0.10$ m flame tube. The six first acoustic eigenmodes calculated without an unsteady flame and different temperatures in each cavity are drawn with dashed lines. The feeding manifold temperature is fixed to $T_1 = 300$ K, while the flame tube is set to $T_2 = 900$ K. Top graph (a) represents the main frequency appearing on the velocity signal spectrum (∘). Lower graph (b) shows the other frequencies found in multiple frequency cases. Two black circles (•) are used in the case of sidebands frequencies (first band of variable amplitude limit cycles) whereas only one circle shows the presence of another mode in the second multiple frequency band. The small arrows indicate the lengths studied and mentioned in the text.

experimental exploration consists of increasing L_1 by steps of 1 cm. Once the maximum extension has been reached the length of the upstream manifold is reduced from $L_1 = 0.77$ m to 0.11 m. Regimes of combustion oscillation are either stable or unstable. In the unstable case, a frequency and amplitude are deduced from pressure, velocity and heat release rate records. In the stable case, the flame does not oscillate and a low level of noise is mainly generated by the fresh stream flowing into the duct.

Oscillatory combustion regimes present different types of limit cycles. One may distinguish two groups. The first features stable oscillation amplitudes which have already been documented in previous articles [8–10,16]. In the second group, one finds GLCs where the oscillation exhibits either regular or irregular envelope modulations. These modulations result from the presence of multiple frequencies which are revealed by a spectral analysis of the signals. One surprising issue is that there is some variability in the limit cycles. The sound signal which is perceived under such conditions has the general character of a "buzzing" but with some irregular quasi-periodic low frequency modulations and it is designated as "buzzing-chugged" combustion.

The configuration used in the present work with a short flame tube exhibits variable amplitude limit cycles in two ranges of length L_1. Fig. 2 shows the frequency evolution obtained by increasing the feeding manifold length L_1 from 0.11 m to 0.77 m. Two graphs display the frequencies corresponding to the major components in the velocity spectrum for each feeding manifold length L_1. The upper graph (Fig. 2(a)) shows the main frequency of the limit cycle whereas the lower graph (Fig. 2(b)) indicates the next most important spectral components in the multiple frequencies cases. When these spectral components are close sidebands of the central frequency the two sideband frequencies are indicated. Otherwise, the lower plot only shows the frequency of the second most important component. An examination of Fig. 2(b), indicates the range of lengths L_1 corresponding to TMLCs, which is embedded between $L_1 = 0.52$ m and 0.64 m. As L_1 is increased from its initial value of 0.11 m, oscillations appear around the first mode and remain in the vicinity of this mode until $L_1 = 0.15$ m. The system then reaches a stable band from $L_1 = 0.16$ m to 0.24 m. At $L_1 = 0.25$ m the system features a new unstable range around the second mode. This single mode oscillation persists until $L_1 = 0.51$ m. A first range of variable amplitude limit cycles is found for $L_1 = 0.40$ m and 0.41 m. In this interval the signal is regularly modulated as shown in Fig. 3, for $L_1 = 0.40$ m. The pressure spectrum features two side peaks located near the main frequency. This side band situation is marked by two black circle symbols plotted in Fig. 2(b). Phase space reconstruction provides some additional insight on the oscillation behavior. The time series analysis [16] requires an embedding dimension d_e and an optimal time delay τ which are then used to plot the trajectories in phase space. The "False Nearest Neighbours" method provides d_e. As explained in [17], the time delay τ may be chosen by examining the signal autocorrelation function and finding the time value where it drops to zero. For $L_1 = 0.40$ m one finds $\tau = 7$ periods of the sampling frequency ($f_s = 16\,384$ Hz), i.e. almost one quarter of the main frequency period found at 600 Hz. The embedding dimension is estimated to be $d_e = 4$. It indicates the need to track the phase portrait in a four-dimensional space. Nevertheless, it would be difficult to follow the trajectory in a such dimension. In this case, it is standard to consider a three-dimensional phase space. In addition, the rate of "false neighbours" is not so high with $d_e = 3$. The "False Nearest Neighbours" technique relies on the points evolution into the phase space when the dimension is progressively increased. When these points are "false neighbours", they move one from another with the increment. This gives a percentage of moving points decreasing along the dimension growth. A rate of 10% is assumed to give the pattern exhibiting the proper dynamical behavior. In the present case, the use of three dimensions is a compromise between the difficulty to read the phase space reconstruction of higher value and the fact that the rate of false nearest neighbours falls to 20% when $d_e = 3$. One obtains a ring like structure confirming that the

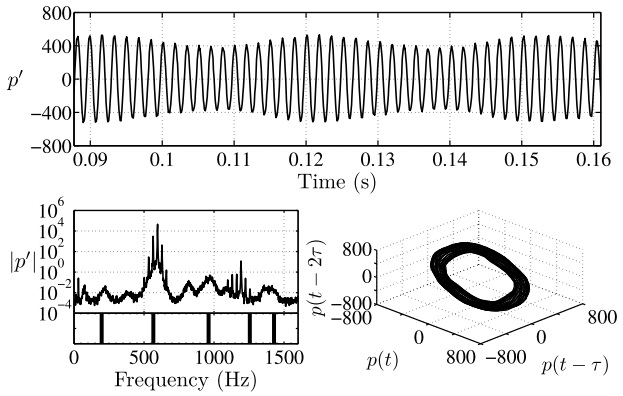

Fig. 3. Pressure evolution recorded by microphone M_2 (top) for $L_2 = 0.10$ m and $L_1 = 0.40$ m. The spectrum (left) and phase space reconstruction (right) are displayed below. Acoustic eigenmodes calculated without the flame but by assuming different temperatures in each cavity are drawn as vertical lines below the pressure spectrum.

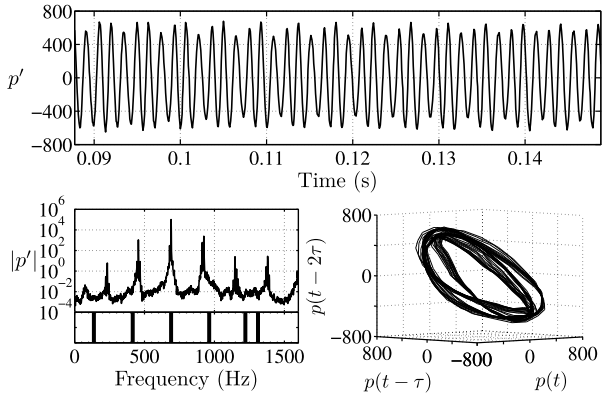

Fig. 4. Pressure evolution recorded by microphone M_2 (top) for $L_2 = 0.10$ m and $L_1 = 0.58$ m. The spectrum (left) and phase space reconstruction (right) are displayed below. Acoustic eigenmodes calculated without the flame but by assuming different temperatures in each cavity are drawn as vertical lines below the pressure spectrum.

amplitude is modulated with a certain steadiness. This pattern features a flat ring which indicates that the frequencies of the different amplitudes are close. In the case of big differences this ring would have not been flat.

Beyond $L_1 = 0.51$ m, the third mode arises until $L_1 = 0.77$ m. This oscillation features multiple frequencies for $L_1 = 0.52$ m to 0.64 m as is well illustrated by analyzing the signal recorded for a particular value of $L_1 = 0.58$ m belonging to this range (Fig. 4). The pressure oscillates at a frequency corresponding to the third mode $f_{m3} = 690$ Hz. Its amplitude is modulated with a period which is equal to three times that corresponding to the fundamental frequency $f_c = f_{m3}$. The spectrum reveals the presence of modes 2 and 3. One also finds a low frequency at 234 Hz which corresponds to the difference between $f_{m3} - f_{m2}$. In the present case this gives rise to a period tripling phenomenon observed in the pressure record where one finds that three fundamental periods are necessary to recover the same signal value. Phase space reconstruction is obtained with the methodology described previously. The embedding dimension $d_e = 4$ while the optimal time delay $\tau = 6$ periods of the sampling frequency f_s, corresponding to 25.3% of the f_{m3} frequency period. A three-dimensional space is used once more and the reconstruction exhibits three circular patterns corresponding to three amplitude levels induced by the period tripling characterizing this case. The phase space reconstruction allows to confirm a different behavior in comparison to the one analyzed before with $L_1 = 0.40$ m. Indeed with $L_1 = 0.58$ m, the circular patterns are not on the same plane. It reveals that the frequency changes largely with the amplitude compared to the previous case. This analysis is especially useful for the other lengths L_1 where the spectrum is not always as clear as the one presented here. It allows one to delineate different circular patterns and helps to clarify the system dynamics.

In a nutshell, this configuration exhibits stable and variable amplitude limit cycles. In the first band of unstable oscillation amplitudes, between $L_1 = 0.40$ m and 0.41 m, the signal is regularly modulated and this corresponds to the presence of two side-peaks around the central frequency. In the second band pertaining to $L_1 = 0.52$ m to 0.64 m, two modes are simultaneously present and generate a frequency difference which in the range of observation produces a period tripling phenomenon. The study is now focused on this second kind of limit cycles sustained by two modes (TMLCs).

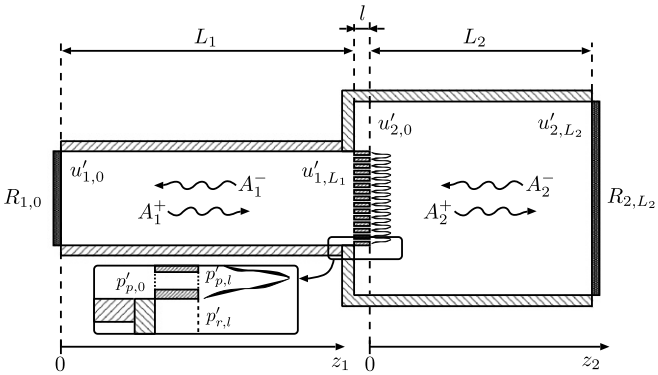

Fig. 5. Burner and symbol convention used for the analytical model.

4. Theoretical interpretation

It is natural to seek an explanation for oscillations of the type described previously. We focus on unstable oscillations sustained by two modes which are probably the most commonly observed in practice. To this purpose we use the FDF framework to determine the growth rates of specific modes of oscillation. The analysis relies on the nonlinear dispersion relation derived by combining an acoustic network description of the system with a flame response represented by a family of transfer functions corresponding to different amplitude levels (the Flame Describing Function).

The model of the system is sketched in Fig. 5. A reflection coefficient defines the inlet and outlet of the combustion system. This can be represented as an acoustic network as in many studies of combustion instability (see [18,19]). A model of the perforated plate, used to anchor small conical flames, is also considered with a dynamical relation adapted from Melling [20] to link the pressure difference and the flow velocity in each channel. By considering boundary and matching conditions of the upstream manifold and flame tube one obtains the following matrix:

$$\begin{pmatrix} 1 & -|R_{1,0}|e^{i\phi_{1,0}} & 0 & 0 \\ 0 & 0 & |R_{2,L_2}|e^{i\phi_{2,L_2}}e^{ik_2L_2} & -e^{-ik_2L_2} \\ \mathcal{A}_1 e^{ik_1L_1} & \mathcal{A}_2 e^{-ik_1L_1} & -1 & -1 \\ \mathcal{B}e^{ik_1L_1} & -\mathcal{B}e^{-ik_1L_1} & \mathcal{C}_1 & \mathcal{C}_2 \end{pmatrix} \begin{pmatrix} A_1^+ \\ A_1^- \\ A_2^+ \\ A_2^- \end{pmatrix} = 0 \tag{2}$$

where $\mathcal{A}_1$, $\mathcal{A}_2$, $\mathcal{B}$, $\mathcal{C}_1$ and $\mathcal{C}_2$ correspond to:

$$\mathcal{A}_1 = 1 + \frac{i\omega l}{\mathcal{P}c_1}\left[1 + \frac{l_v}{r_p}(1+i)\right], \qquad \mathcal{A}_2 = 1 - \frac{i\omega l}{\mathcal{P}c_1}\left[1 + \frac{l_v}{r_p}(1+i)\right]$$

$$\mathcal{B} = \frac{S_1}{S_2}\frac{\rho_2 c_2}{\rho_1 c_1}\left[1 + \left(\frac{T_f}{T_1} - 1\right)Ge^{i\varphi}\right]$$

$$\mathcal{C}_1 = i\left(1 - \frac{S_1}{S_2}\right)\tan(k_2 l) - 1, \qquad \mathcal{C}_2 = i\left(1 - \frac{S_1}{S_2}\right)\tan(k_2 l) + 1$$

In this expression, $|R_{1,0}|\exp(i\phi_{1,0})$ and $|R_{2,L_2}|\exp(i\phi_{2,L_2})$ pertain to the reflection coefficients at the burner inlet and outlet. The FDF appears as $G\exp(i\varphi)$ and T_f denotes the flame temperature. The perforated plate used as a flame holder is taken into account with a model due to Melling [20], where $l_v = (2\nu/\omega)^{1/2}$ stands for the thickness of the acoustic boundary layer in each channel. The porosity appears as $\mathcal{P} = N\pi r_p^2/\pi R_1^2$ where r_p and R_1 respectively designate the radius of a hole of the perforated plate and the one of the feeding manifold. Its surface area is noted S_1 while the one of the confinement tube corresponds to S_2. The determinant of the system must vanish to obtain nontrivial solutions. This provides a dispersion relation (DR) which depends nonlinearly on the amplitude in a way defined by the FDF. The complex angular frequency $\omega = \omega_r + i\omega_i$ solution of the DR gives the angular frequency $\omega_r = 2\pi f$ and the growth rate ω_i of the oscillation. This solution is computed for each length L_1 belonging to the experimental range. This calculation is carried out for different amplitude levels and it is thus possible to follow the solution as a function of the amplitude. By considering all the roots of the dispersion relation for a range of amplitudes and for each feeding manifold length L_1, it is possible to plot the bifurcation diagram shown in Fig. 6 which presents growth rate contours calculated for the first three eigenmodes. The growth rates are displayed with three different colors corresponding to the first three modes as indicated at the top of the figure. Contours plotted in the three domains provide the growth rates as a function of amplitude for each feeding manifold length L_1. When the growth rate vanishes $\omega_i = 0\ \mathrm{s}^{-1}$ one obtains a boundary contour which possibly defines a limit cycle. It is interesting to note at this point that there are regions where a single mode prevails and other regions where there is a modal overlap. When there is an overlap one expects to find a more complex behavior than in the situation featuring an isolated mode.

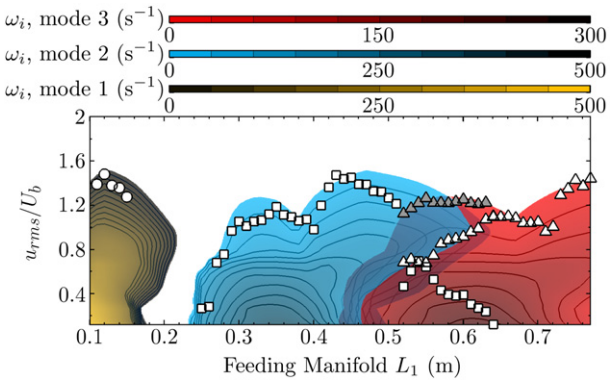

Fig. 6. Growth rate evolution for the $L_2 = 0.10$ m confinement tube and the sweeps of feeding manifold L_1 from 0.11 m to 0.77 m. Three colors are used for each eigenmode. The first is displayed in yellow, the second in blue and the third in red. Scale is given above to graph. Symbols correspond to experiments. ∘ stands for the first mode while □ corresponds to the second one and △ to the third. Gray triangle symbols depict the sum of the 2 modes values in the multiple frequency band ($L_1 = 0.52$ m to 0.64 m).

At this point it is useful to examine the experimentally observed amplitudes of oscillation. The first mode amplitudes are displayed as open circle symbols (∘) while the second mode oscillation amplitudes appear as open square symbols (□). The third mode is represented by open triangle symbols (△), but in the multiple frequency case it is first necessary to separate the components corresponding to the different frequencies. This is accomplished by digital filtering of the record by setting two bandpass filters around the two main frequencies appearing in the power spectrum. This signal filtering is used to display the two modes amplitudes found in the multiple frequency range between $L_1 = 0.52$ m and 0.64 m. It is also interesting to calculate the sum of these two amplitudes without taking into account a possible phase shift. This defines the maximum amplitude which can be reached when the two components are mixed. This amplitude is marked by gray triangle symbols.

In the region where a single mode prevails one finds that the amplitude evolution observed experimentally by changing the feeding manifold length L_1 can be retrieved theoretically by reading this diagram. There is a reasonable match between the experimental points and the amplitude found for a vanishing ω_i. For these points one expects a stable amplitude limit cycle which is indeed observed almost everywhere. The first branches of the oscillation amplitude, i.e. mode 1 and mode 2 between $L_1 = 0.1$ m and 0.51 m, are well predicted. The last part between $L_1 = 0.65$ m and 0.77 m is also fairly well retrieved. There is however a small range of L_1 between 0.40 and 0.41 m where the system features a central frequency and two side bands giving rise to a modulated amplitude at limit cycle. It is possible to show that this particular behavior is related to the dependence of the boundary reflection coefficient with respect to the amplitude level but this will not be examined here. For the stable limit cycle cases the real part of ω provides the oscillation frequency corresponding to the amplitude determined in the bifurcation diagram.

It is now interesting to examine the multiple frequency band between $L_1 = 0.52$ m and 0.64 m. One may first consider that the oscillation would behave as before and that the limit cycle would correspond to $\omega_i = 0$ s^{-1}. If this were so, one would expect a limit cycle around the second mode between $L_1 = 0.52$ m and 0.58 m followed by a limit cycle around the third mode between $L_1 = 0.58$ m and 0.64 m. However, as observed in Fig. 4 for $L_1 = 0.58$ m, the oscillation is not locked on a single frequency. Pressure or velocity records feature two principal frequency components as observed in the power spectrum. By filtering the pressure or velocity signals, one finds that modes 2 and 3 coexist both with a nearly constant amplitude. One then finds that mode 3, represented by open triangle symbols (△), stands for 50% – or more – of the expected oscillation amplitude at $\omega_i = 0$ s^{-1}. This is found by processing the signal in the range $L_1 = 0.55$ m to 0.62 m. Mode 2, represented by open square symbols (□), also appears in this range. Its amplitude is found to be equal to the difference between the value calculated for the limit cycle at $\omega_i = 0$ s^{-1} and the amplitude of mode 3. One can see in Fig. 6 that the combined amplitude of the two modes (gray triangle symbols) closely matches the limit cycle boundary. This phenomenon appears in a case where mode 3 features a supercritical bifurcation (is linearly unstable) while mode 2 has a subcritical bifurcation and is nonlinearly unstable in the range of interest. There is an overlap region where mode 3 has a higher growth rate than mode 2. The third mode amplitude dominates that of the second mode but the third mode does not take over and oscillations at the second mode frequency persist. There is a crossing point in amplitudes which corresponds to coinciding growth rates of the two modes.

In addition to the growth rate ω_i it is interesting to examine the corresponding values of the angular frequency ω_r. Fig. 7 displays the frequency calculated from the dispersion relation at the limit cycle amplitude predicted by reading the bifurcation diagram. The frequencies are compared with experimental values plotted as symbols. Open circle symbols (∘) correspond to the first mode frequencies while the second and the third modes are respectively displayed by means of open square (□) and open triangle symbols (△). Predictions corresponding to $\omega_i = 0$ s^{-1} are plotted as dark bold lines, whereas frequencies calculated in the multiple frequency cases are displayed as light gray bold lines. In this last condition, mode 2 and mode 3 frequencies are read at the amplitude where growth rates intersect.

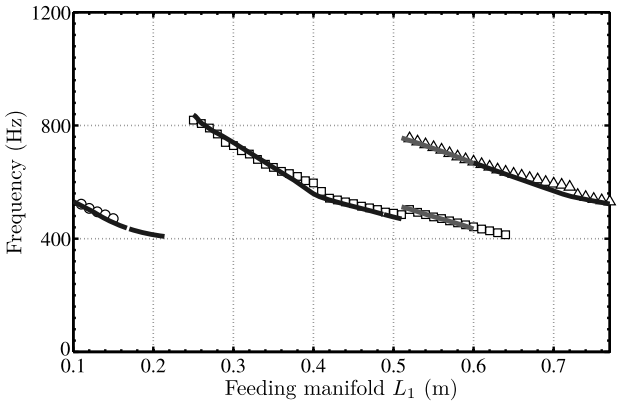

Fig. 7. Theoretical and experimental frequency at limit cycle. Open circle symbols (○) are linked to the first mode while the second mode appears as open square symbols (□) and the third mode as open triangle symbols (△). The dark bold lines represent predictions for $\omega_i = 0\ s^{-1}$ whereas the gray ones correspond to the frequencies of the two modes limit cycles.

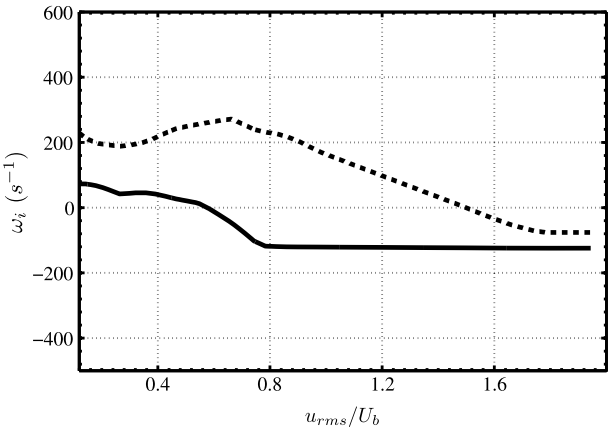

Fig. 8. Theoretical growth rate trajectories calculated with the FDF for the $L_2 = 0.10$ m confinement tube and $L_1 = 0.45$ m. The dashed line (- -) indicates the second mode growth rates whereas the bold line (–) corresponds to the third mode.

The multiple frequency cases clearly arise from a combination of two modes. In addition one finds that the frequencies mix and produce a signal with a difference frequency which is reminiscent of a similar situation found in wireless telecommunications where it is designated as frequency "heterodyning". Heterodyning gives rise to the sum or difference of the two original frequencies input in a nonlinear system. There are some theoretical calculations indicating the possibility of double mode oscillations. For example, Culick and his co-workers [21], show that this can happen if two modes exist of which one is stable and the other is unstable. This is only found for certain ranges of values of the growth rates but has not been observed in the present experiments and the double mode of oscillation arises when some other conditions are fulfilled as explained in what follows.

To predict the occurrence of multi-mode oscillations, it is natural to examine growth rate trajectories and derive conditions which gives rise to this behavior. First, it is found that dual mode oscillations appear when there is a modal overlap i.e. when the regions of positive growth rates of two modes intersect. A detailed examination reveals two types of overlap. The first type corresponds to two linearly unstable modes as shown in Fig. 6 between $L_1 = 0.43$ m and 0.48 m. In this case, exemplified in Fig. 8 for $L_1 = 0.45$ m, the second mode dominates over the whole amplitude range. By reading the bifurcation diagram, one expects that the oscillation will be locked on the mode which has the highest growth rate. This is well observed experimentally and in the corresponding range the second mode of oscillation prevails with an amplitude which closely matches that determined from the FDF calculation. It is well verified in this case that the third mode does not arise in the power spectrum. This kind of modal overlap has already been considered in previous calculations and experiments which all confirm that the mode with the highest growth rate values is dominant. For example, in [15] two linearly unstable modes exist for a short flame tube of 0.10 m and a feeding manifold length L_1 between 0.28 m and 0.38 m (see Fig. 8 in [15]). In this range, the second mode takes over and oscillations at the limit cycle correspond to a single frequency.

The second type of overlap is found in the present experiments when $L_1 > 0.48$ m, in the range where the second mode becomes nonlinearly unstable while the third mode is linearly unstable. In this range, the two modes are sustained. The existence of linearly and nonlinearly unstable modes is a necessary condition for a dual mode of oscillation but this is not

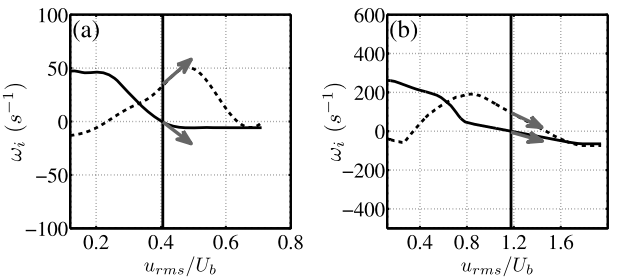

Fig. 9. Theoretical growth rate trajectories calculated with the FDF. The dashed line (--) shows the second mode growth rate whereas the bold line (–) corresponds to the third mode. (a) pertains to calculations from previous work [10] for $L_1 = 0.54$ m and a confinement tube of $L_2 = 0.10$ m. In this case, the crossing of trajectories leads to a mode switching during the growth of oscillation. (b) is obtained from the present investigation at $L_1 = 0.52$ m with the $L_2 = 0.10$ m confinement tube. Experiments reveal a dual mode oscillation. The first trajectory crossing $\omega_i = 0$ is indicated by means of a vertical line. Gray arrows at this point represent the tangent lines and provide the signs of the slopes for the two modes.

sufficient. Indeed, previous experiments indicate that when this condition is verified the two modes do not always persist simultaneously. In the unconfined geometry discussed in [8] and in the confined configuration explored in [10] it was found that the oscillation begins at the third mode frequency and that as the amplitude increases mode switching takes place and the second mode prevails. The final outcome is a limit cycle corresponding to a vanishing growth rate of the nonlinearly unstable mode ($\omega_i = 0\ s^{-1}$). It is then necessary to find the additional condition which distinguishes situations where a single mode takes over from that where the two modes are sustained. This is accomplished by examining the growth rate trajectories obtained by plotting this quantity with respect to the amplitude of oscillation.

An example is given in Fig. 9 which shows two configurations where the trajectory of a linearly unstable mode (LUM) crosses that of a nonlinearly unstable mode (NLUM). The first case examined in Fig. 9(a) corresponds to experiments reported previously [10] in which mode switching was observed and predicted for different operating conditions. The second case, shown in Fig. 9(b), pertains to the present investigation for $L_1 = 0.52$ m. The amplitude level where the linearly unstable mode (LUM) trajectory crosses the horizontal axis $\omega_i = 0$ is plotted as a vertical bold line in these two diagrams. Two arrows denote the tangent lines to the growth rate trajectories at this particular amplitude level designated as a_0. In the case shown in Fig. 9(a) which gives rise to mode switching, the slope of the third mode (LUM) growth rate is negative while the slope of the second mode (NLUM) growth rate is positive:

$$(d\omega_{i3}/da)_{a_0} < 0 \quad \text{and} \quad (d\omega_{i2}/da)_{a_0} > 0 \tag{3}$$

In contrast, when the two modes are simultaneously sustained, the growth rate slopes are both negative as illustrated in Fig. 9(b):

$$(d\omega_{i3}/da)_{a_0} < 0 \quad \text{and} \quad (d\omega_{i2}/da)_{a_0} < 0 \tag{4}$$

The present experiments indicate that when there is a modal overlap involving a linearly unstable mode (LUM) and a nonlinearly unstable mode (NLUM) and when condition (4) is satisfied the oscillation takes place at the two frequencies. On the other hand, when condition (3) is satisfied, mode switching takes place and the nonlinearly unstable mode prevails.

By applying the previous criterion it is possible to delineate the region where one expects oscillations at two modal frequencies. This can be simply done by calculating the growth rate differentials with respect to the amplitude in the region of modal overlap. The region where the criterion has to be satisfied appears in gray in Fig. 10. For $L_1 < 0.50$ m the first condition on the existence of linearly and nonlinearly unstable modes is not fulfilled. Condition (4) is satisfied for $0.50 \leqslant L_1 \leqslant 0.61$ m and one expects to find a double mode oscillation. The boundaries of this range nearly match that found in the experiment which is located between 0.52 m and 0.64 m. Except for this small difference due to uncertainties in the FDF determination, the criterion stated previously suitably provides the range where two modes are sustained simultaneously.

In summary, it appears that double mode oscillations can be expected when a linearly and a nonlinearly unstable modes overlap and when in addition condition (4) on the rates of change of the growth rates is satisfied.

5. Conclusion

Thermo-acoustic coupling is investigated in a generic combustion system featuring a feeding manifold, a multipoint injector and a small length flame tube confining the combustion region. Two classes of limit cycle have been identified. The first features a nearly stable oscillation amplitude, whereas the second shows an amplitude unsteadiness. These variations are of different kinds. In the present experiment, two types arise indicating that TMLCs can occur in different parametric ranges. The present study concentrates on a range of parameters where oscillations are sustained by two modes also giving rise to frequency mixing. In this range the limit cycle is regularly distorted via a low frequency formed by heterodyning. It is shown that such a process can be expected by examining FDF calculations. It is first observed that a nonlinear dispersion relation including a flame describing function provides predicted amplitudes and frequencies which are in good agreement

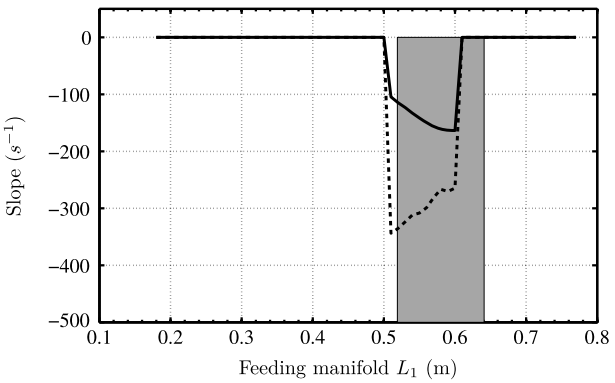

Fig. 10. Rates of change (slope) of the growth rates corresponding to mode 2 (dashed line - -) and mode 3 (bold line –). The calculation is carried out in the region of overlap of the LUM and NLUM. Slope of each mode is determined at the amplitude where the linearly unstable mode (LUM) crosses $\omega_i = 0$. Gray area indicates the lengths where dual mode oscillation has been found in the experiment.

with experimental values for stable limit cycle cases. In the TMLC cases, a double mode oscillation is shown to occur when two conditions are fulfilled. The first condition is an overlap between a supercritical bifurcation mode (LUM) and a subcritical bifurcation mode (NLUM). The second condition requires that the slopes of growth rate trajectories of these two modes have negative signs at the point where the LUM would reach its limit cycle. In contrast when the signs of these slopes are distinct, i.e. the slope of the NLUM growth rate is positive, mode switching takes place and a single mode prevails at the limit cycle.

Acknowledgements

The research leading to these results has received funding from the European Community's Seventh Framework Programme (FP7/2007-2013) under Grant Agreement # ACP8-GA-2009-234009. This is part of the 4-year KIAI project started in May 2009, which is a European initiative financed under the FP7 and addresses innovative solutions for the development of new combustors in aero-engines. It aims at providing low NOx methodologies to be applied to design these combustors.

We also wish to thank J. Beaunier and Y. Le Teno for the technical support provided to this research.

References

[1] N. Noiray, D. Durox, T. Schuller, S. Candel, Self-Induced instabilities of premixed flames in a multiple injection configuration, Combust. Flame 145 (3) (2006) 435–446.
[2] B. Schuermans, F. Guethe, D. Pennell, D. Guyot, C.O. Paschereit, Thermoacoustic modeling of a gas turbine using transfer functions measured under full engine pressure, J. Eng. Gas Turb. Power 132 (11) (2010) 111503.
[3] T. Poinsot, D. Veynante, F. Bourienne, S. Candel, E. Esposito, J. Surget, Initiation and suppression of combustion instabilities by active control, Proc. Combust. Inst. 22 (1) (1989) 1363–1370.
[4] W. Lang, Harmonic frequency generation by oscillating flames, Combust. Flame 83 (3–4) (1991) 253–262.
[5] A.P. Dowling, Nonlinear self-excited oscillations of a ducted flame, J. Fluid Mech. 346 (1997) 271–290.
[6] P.J. Langhorne, Reheat buzz: an acoustically coupled combustion instability. Part 1. Experiment, J. Fluid Mech. 193 (1988) 417–443.
[7] A.P. Dowling, A kinematic model of a ducted flame, J. Fluid Mech. 394 (1) (1999) 51–72.
[8] N. Noiray, D. Durox, T. Schuller, S. Candel, A unified framework for nonlinear combustion instability analysis based on the flame describing function, J. Fluid Mech. 615 (2008) 139–167.
[9] P. Palies, D. Durox, T. Schuller, S. Candel, Nonlinear combustion instability analysis based on the flame describing function applied to turbulent premixed swirling flames, Combust. Flame 158 (10) (2011) 1980–1991.
[10] F. Boudy, D. Durox, T. Schuller, S. Candel, Nonlinear mode triggering in a multiple flame combustor, Proc. Combust. Inst. 33 (Part 1) (2011) 1121–1128.
[11] E.H. Dowell, R. Clark, A Modern Course in Aeroelasticity, Springer, 2004.
[12] J.D. Sterling, Nonlinear analysis and modelling of combustion instabilities in a laboratory combustor, Combust. Sci. Technol. 89 (1–4) (1993) 167–179.
[13] L. Kabiraj, R.I. Sujith, P. Wahi, Experimental studies of bifurcations leading to chaos in a laboratory scale thermoacoustic system, in: Proceedings of the ASME Turbo Expo 2011, GT2011-46149, Vancouver, British, Columbia, Canada, 2011.
[14] L. Kabiraj, R.I. Sujith, Investigation of subcritical instability in ducted premixed flames, in: Proceedings of the ASME Turbo Expo 2011, GT2011-46155, Vancouver, British, Columbia, Canada, 2011.
[15] F. Boudy, D. Durox, T. Schuller, G. Jomaas, S. Candel, Describing function analysis of limit cycles in a multiple flame combustor, J. Eng. Gas Turb. Power 133 (6) (2011).
[16] M. Small, Applied Nonlinear Time Series Analysis: Applications in Physics, Physiology and Finance, World Scientific Publ., 2005.
[17] H.D.I. Abarbanel, R. Brown, J.J. Sidorowich, L.S. Tsimring, The analysis of observed chaotic data in physical systems, Rev. Modern Phys. 65 (4) (1993) 1331–1392.
[18] J.J. Keller, Thermoacoustic oscillations in combustion chambers of gas turbines, AIAA J. 33 (12) (1995) 2280–2287.
[19] C.O. Paschereit, P. Flohr, B. Schuermans, Prediction of combustion oscillations in gas turbine combustors, in: AIAA Paper 2001-0484, Reno, Nevada, US, 2001.
[20] T.H. Melling, The acoustic impedance of perforates at medium and high sound pressure levels, J. Sound Vib. 29 (1) (1973) 1–65.
[21] E. Awad, F.E.C. Culick, On the existence and stability of limit cycles for longitudinal acoustic modes in a combustion chamber, Combust. Sci. Technol. 46 (3–6) (1986) 195–222.